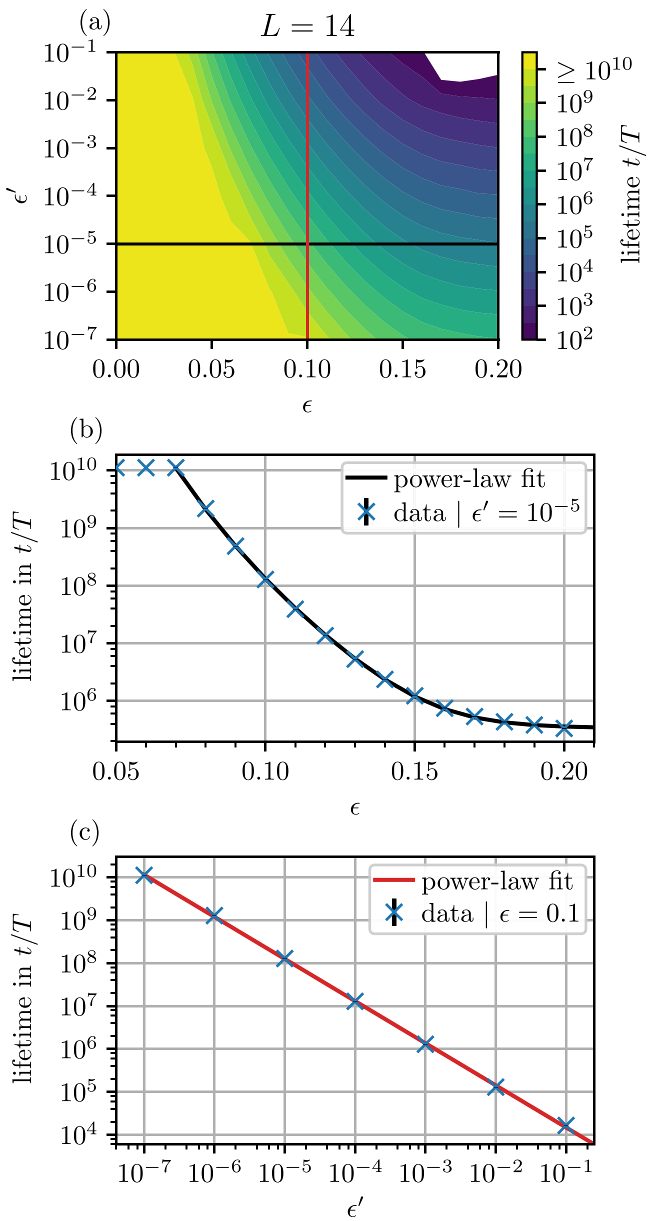

FIG. 3. The lifetime of the global z magnetization $\langle \sum_i \sigma_z^i \rangle / L$ for a range of drive deviation parameters ϵ and ϵ' including a metronome spin on one boundary site is shown in (a). (b) A horizontal cut through this plane at fixed $\epsilon' = 10^{-5}$. (c) A vertical cut at fixed $\epsilon = 0.1$, as indicated by the black and red lines in (a), respectively. All data points have been obtained through cosine fits, as shown in Fig. 2. Lifetimes above $t = 10^{10}T$ and below $t = 10^2 T$ cannot be adequately resolved and are therefore exempt from the fit.

which yields the observed difference for the values used of $\epsilon = 0.1$ and $\epsilon' = 10^{-5}$.

Next, we systematically investigate the dependence of the global magnetization lifetime T_R on the deviations of the drive angle. For this, we repeat the procedure explained above for a number of combinations of the values of ϵ and ϵ'. The results are shown in Fig. 3(a), where we have probed a wide regime of drive parameters. At small ϵ, we observe lifetimes that exceed the resolved duration of 10^{10} Floquet cycles (yellow region). For fixed $\epsilon = 0.1$, we find that T_R is approximately inversely proportional to ϵ', $T_R \propto (\epsilon')^\alpha$ with $\alpha = -0.982 \pm 0.007$, as shown in Fig. 3(b), which is consistent with the reasoning presented in Eq. (6). For fixed $\epsilon' = 10^{-5}$, the recorded lifetimes follow a power law with offset, $T_R/T \approx a\epsilon^\beta + (3.35 \pm 0.09)10^5$, with $\beta = -12.29 \pm 0.03$. This value of β roughly agrees with the expectation $\beta = -13$ implied by Eq. (6). However, the observed convergence to a nonzero lifetime in the limit of large ϵ is not predicted by this perturbative picture [cf. Eq. (6)].

This behavior can be understood by taking $\epsilon' \to 0$. In this limit, the dynamics of the metronome spin effectively decouple from the bulk of the chain, since the metronome cannot leave the manifold of $\{|\uparrow\rangle, |\downarrow\rangle\}$, alternating between the two states in every Floquet cycle. One can now write down a Hamiltonian restricted to the bulk of the chain, where the coupling between the metronome and its neighboring spin, $s_z^1 s_z^2$, can be replaced by an effective field on the second spin of the chain,

$$H_{F,\mathrm{bulk}}^{(0)} = \frac{1}{T}\left(\tilde{h} s_z^2 + t_1 \sum_{i=2}^{L-1} J_{i,i+1} s_z^i s_z^{i+1} - \pi \sum_{i=2}^{L} \epsilon_i s_x^i\right). \quad (7)$$

The new field term effectively breaks the spin-flip symmetry of the original Hamiltonian $H_F^{(0)}$ in the bulk and thus introduces an energy gap between the two polarized states. Therefore, the prepared polarized state is no longer the superposition of the two lowest-energy eigenstates but, rather, very close to the lowest eigenstate of $H_{F,\mathrm{bulk}}^{(0)}$, resulting in a stable magnetization plateau. For cases where $\epsilon' \ll 1$ the metronome spin stays close to the $\{|\uparrow\rangle, |\downarrow\rangle\}$ manifold for extended periods of time before it and, subsequently, the rest of the chain dephases. However, in the large ϵ limit, large parts of the chain farther away from the metronome lose their magnetization much earlier due to domain-wall excitations. Still, since the metronome is largely decoupled in its dynamic from the rest of the chain, it retains nonvanishing magnetization even at late times, keeping the magnetization plateau alive, albeit at a lower value $\langle \sum_i \sigma_z^i \rangle / L \sim \mathcal{O}(1/L)$. This explains the observed saturation behavior in the lifetime dependence at large ϵ in Fig. 3(b).

B. Edge-mode enhancement for random bit-string initial states

Next, we investigate how the introduction of a metronome affects the dynamics of different initial states beyond the fully polarized case. To this end, we subject an ensemble of random bit-string states, i.e., states where every spin is either $|\uparrow\rangle$ or $|\downarrow\rangle$ chosen randomly, to the Floquet sequence given in Eq. (1). As the magnetization of these states vanishes on average, we instead consider local magnetization autocorrelators in the rotating frame, $\langle \sigma_z^i(0)\sigma_z^i(t/T)\rangle(-1)^{\lfloor t/T \rfloor} =: Z_i$. Three autocorrelators of selected spin sites, averaged over a set of 500 bit-string initial states, are shown in Fig. 4. The three panels show the autocorrelators of the metronome spin on the site $i = 1$ in Fig. 4(a), of a spin in the bulk of the chain on site $i = 8$ in Fig. 4(b), and at the other chain boundary on site $i = 14$ in Fig. 4(c).

First, the results for the autocorrelator of the metronome spin itself are in line with the results for the metronome single-spin magnetization in Fig. 2 (right axis). The